Free Material Optimization: Towards the Stress Constraints*

Dedicated to Pauli Pedersen on the occasion of his 70th birthday

Michal Kočvara‡ and Michael Stingl**

Abstract

Free material design deals with the question of finding the lightest structure subject to one or more given loads when both the distribution of material and the material itself can be freely varied. We additionally consider constraints on local stresses in the optimal structure. We discuss the choice of formulation of the problem and the stress constraints. The chosen formulation leads to a mathematical program with matrix inequality constraints, so-called nonlinear semidefinite program. We present an algorithm that can solve these problems. The algorithm is based on a generalized augmented Lagrangian method. A number of numerical examples demonstrates the effect of stress constraints in free material optimization.

1 Introduction

The goal of the paper is to find a formulation of stress constraint in the free material optimization (FMO) problem that would be computationally tractable and would lead to reasonable and expected results. The underlying FMO model was introduced in [3] and later developed in [15] and [2]. The design variable is the full elastic stiffness tensor that can vary from point to point; it should be physically available but is otherwise not restricted. This problem gives the best physically attainable material and can be considered the "ultimate" generalization of the structural optimization problem.

The standard FMO problem (as well as the standard topology optimization problem like SIMP) deals with compliance and "weight" (the term weight in FMO is somewhat subtle; see the next section). We either minimize the weight subject to compliance

*This research was supported by the Academy of Sciences of the Czech Republic through grant No. A1075402.

‡Institute of Information Theory and Automation, Academy of Sciences of the Czech Republic, Pod vodárenskou věží 4, 18208 Praha 8 and Czech Technical University, Faculty of Electrical Engineering, Technická 2, 166 27 Prague 6, Czech Republic, kocvara@utia.cas.cz.

**Institute of Applied Mathematics, University of Erlangen-Nuremberg, Martensstrasse 3, 91058 Erlangen, Germany, stingl@am.uni-erlangen.de.

constraint or vice versa. However, in engineering practise, it is usually the local stress or strain that should be controlled. One of the most often causes of structural failure is high stress, so it is desirable to keep it within given limits during the optimization process.

To control the stress in material and topology optimization is, however, not an easy task; see, e.g., [6] or [11]. The first problem to be faced is how to measure stress, i.e., what kind of failure criteria should be used. This question is even more complicated in the FMO case when we design the material itself (see the introduction of Section 3). In this article we opted for a (local) integral measure of the norm of the stress tensor. A-posteriori, we also compute other standard failure criteria, in order to see the effect of the chosen constraint on these. The second problem is technical. Writing down, formally, the optimization problem with, say, constraints on the von Mises stress, we will get a difficult mathematical program that is almost impossible to solve by available optimization software (we are talking about reasonably large dimensions). It is often a problem with so-called vanishing constraints ([1]) and/or problem that does not satisfy standard constraint qualifications. Again, the situation is even more complicated in the FMO case, because the variables are matrices (the discretized elastic stiffness tensor) and vectors (displacements) that appear in the constraints in a nonlinear way. Hence we face a nonlinear (nonconvex) semidefinite programming problem.

In Section 4 we present an algorithm that can deal with these problems. It is based on the generalized augmented Lagrangian method described and analyzed in [8, 12]. However, in order to solve the particular problems of FMO with stress constraints, we had to perform several substantial modifications of the existing algorithm and thus finished with a new one.

After introducing the basic model, we compare several models of the stress and strain constrained problem by means of a benchmark numerical example, the L-shaped domain. In particular, we compare the FMO problem with the (easier) variable thickness sheet (VTS) problem and show that the VTS problem cannot serve as a substitute for FMO. We also show that the strain constraints, being too restrictive, typically lead to false or suboptimal results and that it is advisable (both in the VTS and FMO context) to use the stress constraints. The VTS and FMO results with stress constraints lead to significant change of the design, compared to unconstrained solution. In the VTS case, the stress is controlled by the change of geometry around the re-entrant corner. In the FMO case, the change is rather on the level of material properties.

2 Primal FMO problem

2.1 Setting of the problem

Material optimization deals with optimal design of elastic structures, where the design variables are material properties. The material can even vanish in certain areas, thus one often speaks of topology optimization.

Let $\Omega \subset \mathbb{R}^2$ be a two-dimensional bounded domain[1] with a Lipschitz boundary. By

[1]The entire presentation is given for two-dimensional bodies, to keep the notation simple. Analogously, all this can be done for three-dimensional solids.

$u(x) = (u_1(x), u_2(x))$ we denote the displacement vector at a point x of the body under load f, and by

$$e_{ij}(u(x)) = \frac{1}{2}\left(\frac{\partial u_i(x)}{\partial x_j} + \frac{\partial u_j(x)}{\partial x_i}\right) \quad \text{for } i,j = 1,2$$

the (small-)strain tensor. We assume that our system is governed by linear Hooke's law, i.e., the stress is a linear function of the strain

$$\sigma_{ij}(x) = E_{ijk\ell}(x)e_{k\ell}(u(x)) \qquad \text{(in tensor notation)},$$

where E is the elastic stiffness tensor. The symmetries of E allow us to interpret the 2^{nd} order tensors e and σ as vectors

$$e = (e_{11}, e_{22}, \sqrt{2}e_{12})^T \in \mathbb{R}^3,\ \sigma = (\sigma_{11}, \sigma_{22}, \sqrt{2}\sigma_{12})^T \in \mathbb{R}^3.$$

Correspondingly, the 4^{th} order tensor E can be written as a symmetric 3×3 matrix

$$E = \begin{pmatrix} E_{1111} & E_{1122} & \sqrt{2}E_{1112} \\ & E_{2222} & \sqrt{2}E_{2212} \\ \text{sym.} & & 2E_{1212} \end{pmatrix}. \tag{1}$$

In this notation, Hooke's law reads as $\sigma(x) = E(x)e(u(x))$.

For the elastic stiffness tensor E and a given external load function $f \in [L_2(\Gamma)]^2$ (where Γ is the part of boundary of Ω that is not fixed by Dirichlet boundary conditions) the system is in equilibrium for a displacement function u which solves the weak equilibrium equation

$$\int_\Omega \langle E(x)e(u(x)), e(v(x))\rangle \mathrm{d}x - \int_\Gamma f(x)\cdot v(x)\mathrm{d}x, \quad \forall v \in \mathscr{V} \tag{2}$$

where $\mathscr{V} \subset [H^1(\Omega)]^2$ reflects the Dirichlet boundary conditions.

In *free material optimization* (FMO), the design variable is the elastic stiffness tensor E which is a function of the space variable x (see [3]). The only constraints on E are that it is physically reasonable, i.e., that E is symmetric and positive semidefinite. As a "cost" of E we use the trace of E. The *minimum weight single-load FMO problem* reads as

$$\max_{u\in\mathscr{V},\ E\in L^\infty(\Omega)} \int_\Omega \mathrm{Tr}(E)\mathrm{d}x \tag{3}$$

subject to

$$E \succeq 0$$
$$\underline{\rho} \le \mathrm{Tr}(E) \le \overline{\rho}$$
$$u \text{ solves (2)}$$
$$\int_\Gamma f(x)\cdot u(x)\mathrm{d}x \le \gamma.$$

The last (compliance) constraint guerantees that the resulting structure is capable of carrying the given force.

2.2 Discretization

Let m denote the number of finite elements and n the number of nodes. We approximate the matrix function $E(x)$ by a function that is constant on each element, i.e., characterized by a vector of matrices $E = (E_1, \ldots, E_m)$ of its element values. We further assume that the displacement vector $u(x)$ is approximated by a continuous function that is bilinear on every element. Such a function can be written as $u(x) = \sum_{i=1}^{n} u_i \vartheta_i(x)$ where u_i is the value of u at i-th node and ϑ_i is the basis function associated with i-th node (for details, see [4]). At each node the displacement has 2 components, so $u \in \mathbb{R}^{2n}$. With the basis functions ϑ_j, $j = 1, \ldots, n$, we define (3×2) matrices

$$\widehat{B}_j = \begin{pmatrix} \frac{\partial \vartheta_j}{\partial x_1} & 0 \\ 0 & \frac{\partial \vartheta_j}{\partial x_2} \\ \frac{1}{2}\frac{\partial \vartheta_j}{\partial x_2} & \frac{1}{2}\frac{\partial \vartheta_j}{\partial x_1} \end{pmatrix}.$$

Now, for the i-th finite element, let $\mathscr{D}_i$ be an index set of nodes belonging to this element. Let *nig* denotes the number of Gauss integration points in each element. By $B_{i,k}$ we denote the block matrix composed of (3×2) blocks $\widehat{B}_j$ at the j-th position, $j \in \mathscr{D}_i$, (evaluated at the k-th integration point) and zeros otherwise. Hence the full dimension of $B_{i,k}$ is $(3 \times 2n)$.

The (global) stiffness matrix A is a sum of element stiffness matrices A_i:

$$A(E) = \sum_{i=1}^{m} A_i(E), \quad A_i(E) = \sum_{k=1}^{nig} B_{i,k}^T E_i B_{i,k}.$$

After the discretization, problem (3) becomes

$$\begin{aligned} &\min_{u,E} \sum_{i=1}^{m} \mathrm{Tr}(E_i) \qquad (4) \\ &\text{subject to} \\ &\quad E_i \succeq 0, \quad i = 1, \ldots, m \\ &\quad \underline{\rho} \le \mathrm{Tr}(E_i) \le \overline{\rho} \quad i = 1, \ldots, m \\ &\quad f^T u \le \gamma \\ &\quad A(E)u = f. \end{aligned}$$

Problem (4) is a mathematical programming problem with linear matrix inequality constraints and standard nonlinear constraints; this is the so-called nonlinear semidefinite programming (NSDP) problem. Recently, there is not much software available for these problems. In Section 4 we will present two modifications of an augmented Lagrangian algorithm used in our software package PENNON that can be used to the solution of NSDP problems of type (4).

However, it was shown in [3] (see also [15] and [10]) that (4) is equivalent to the

variable thickness sheet (VTS) problem

$$\begin{aligned} &\min_{u,\rho} \sum_{i=1}^{m} \rho_i \qquad (5)\\ &\text{subject to}\\ &\quad \underline{\rho} \le \rho_i \le \overline{\rho} \quad i = 1,\dots,m\\ &\quad f^T u \le \gamma\\ &\quad \sum_{i=1}^{m} \rho_i A_i(E_0) u = f\,, \end{aligned}$$

with elastic stiffness tensor $E_0 = I$ (identity matrix), where the variable ρ is the thickness in the VTS problem and gives us the trace of optimal E in the equivalent FMO problem (4).

Now, (5) can be equivalently formulated as a convex optimization problem with linear objective and quadratic constraints (see again [15]):

$$\begin{aligned} &\min_{u,\alpha,\beta\ge 0,\delta\ge 0} \alpha - 2f^T u + \overline{\rho}\sum_{i=1}^{m}\beta_i - \underline{\rho}\sum_{i=1}^{m}\delta_i \qquad (6)\\ &\text{subject to}\\ &\quad u^T\left(\sum_{k=1}^{nig} B_{i,k}^T E_0 B_{i,k}\right) u \le \alpha + \beta_i - \delta_i \quad i = 1,\dots,m\,. \end{aligned}$$

This problem can be solved very efficiently by recent interior point codes (e.g., [14, 13]) or by a generalized augmented Lagrangian approach ([8]).

3 Stress constraint

In engineering practise, it is not (only) the compliance but some measure of local strain that should be controlled. One of the most often causes of structural failure is high stress, so it is desirable to keep it within given limits during the optimization process.

This, however, is not an easy task. First, when designing general anisotropic material, it is unclear what kind of stress measure (failure criterion) to take. To a great extent, this depends on the realization of the optimal result: should the material be manufactured as fibrous composite, a laminate, by tape-laying procedure, should it be just approximated by isotropic material with reinforcement—all these technologies use different failure criteria which are sometimes not even well understood. We, however, do not want to limit ourselves to a particular manufacturing procedure in this phase, rather to keep the design process as general as possible. Hence we decided to evaluate the stress by a norm of the stress (or strain) tensor, integrated over the finite element. In the postprocessing phase, we also compute other standard failure criteria to see the effect on those. Another reason why to take this particular measure of stress is to keep the problem computationally tractable. This is, in fact, the second reason why there are not many successful approaches to stress constraints reported in the literature. Stress

constraints, added to topology or material design problem, lead to hard optimization problems with so-called vanishing constraints ([1]) and/or problems that do not satisfy standard constraint qualifications and are thus very difficult to solve by common software of mathematical programming.

In the continuous formulation, we would work with pointwise stresses, i.e., we would restrict the norm $\|\sigma(x)\|$ for all $x \in \Omega$. However, in the finite element approximation we use the primal formula (working with displacements) and it is a well-known fact that, generally, evaluation of stresses (from displacements) at points may be rather inexact. Hence we will consider the following integral form of stress and strain constraints

$$\int_{\Omega_i} \|\sigma\|^2 \le s_\sigma |\Omega_i| \quad \text{and} \quad \int_{\Omega_i} \|e\|^2 \le s_e |\Omega_i| \,; \tag{7}$$

here Ω_i is the i^{th} finite element and $|\Omega_i|$ its volume. The integrals will be further approximated by the Gaussian intergation formulas, as in the finite element interpolation. To simplify the notation, in the following, we will skip the multiplication by the volume $|\Omega_i|$ and consider it included in the upper bounds s_σ or s_e; in all numerical examples we will use elements of the same volume, so this should not lead to any misuderstanding.

3.1 VTS with stress and strain constraints

Let us first consider the variable thickness sheet problem (5). The simplest modification is to add here strain constraints to get:

$$\begin{aligned}
&\min_{u,\rho} \sum_{i=1}^{m} \rho_i && (8)\\
&\text{subject to}\\
&\quad \underline{\rho} \le \rho_i \le \overline{\rho} \quad i = 1,\dots,m\\
&\quad f^T u \le \gamma\\
&\quad \sum_{i=1}^{m} \rho_i A_i(E_0) u = f\\
&\quad \sum_{k=1}^{nig} \|B_{i,k} u\|^2 \left[= u^T \left(\sum_{k=1}^{nig} B_{i,k}^T B_{i,k} \right) u \right] \le s_e,\ i = 1,\dots,m\,.
\end{aligned}$$

Here we added to the original problem a set of convex quadratic constraints, so we would not expect the new problem to be any harder than the original one.

Remark 3.1 Note that when we consider the dual VTS problem (6) with $E = I$, set $\underline{\rho} = 0$ and neglect the upper bound on ρ, we get the problem

$$\begin{aligned}
&\min_{u,\alpha} \alpha - f^T u && (9)\\
&\text{subject to}\\
&\quad u^T \left(\sum_{k=1}^{nig} B_{i,k}^T B_{i,k} \right) u \le \alpha \quad i = 1,\dots,m\,.
\end{aligned}$$

So the VTS problem (9) as such *is* a problem with strain constraints. Moreover, the vector of Lagrangian multipliers associated with the inequality constraints at the optimal point (u^*, α^*) is just the optimal primal vector ρ^* in formulation (5); see [15]. It is readily seen that when a constraint is active, the strain in the corresponding element is on its upper bound; on the other hand, when a constraint is inactive, the multiplier is equal to zero and the corresponding element is not present in the optimal structure. We thus get a *fully strained design*, where the strains are measured by the integral over the element of the square of the norm of the strain tensor.

In all figures below, we use the color scale shown in Fig. 1. Here the red color indicates the maximal and violet the minimal value plus some epsilon. When the minimal value is zero, it is depicted as white. All examples presented below were solved by

Figure 1: Color scale used in all figures; red indicates maximal and violet almost minimal value; the minimal value is white.

the code PENNON described in Section 4, in particular, by the modification given in Section 4.2.

Example 3.2 The classic example for testing the effect of stress constraints is the L-shaped domain; see Fig. 2(left). When made of homogeneous isotropic material, the structure has a stress concentration at the peak of the re-entrant corner. If we transform the problem to a local radial coordinate system, located at this corner, the radial stress components would go to infinity when aproaching the origin. In the global Cartesian coordinate system, the norm of the stress tensor goes to infinity as we approach the re-entrant corner. When we solve the discretized problems with a homogeneous mesh, the stress would only go to infinity when the mesh size parameter goes to zero. For fixed mesh size, however, the stress values still reach much bigger values at the elements neighboring the corner than in the rest of the domain. For the VTS problem (where the material properties are fixed and we just design the ρ), the only way to remove the stress singularity is to change the geometry of the domain, in particular, to replace the sharp corner by a sort of smooth arc.

For this and all the subsequent examples we will consider discretization of the domain by 7500 finite elements (squares) of the same size. When we solve the VTS problem (6) with an isotropic material E_0 characterized by Young's modulus 1.0 and Poison ration 0.3, we obtain the result presented in Fig. 2(right) (to simplify the presentation, and to get a well-conditioned problem, we scale Young's modulus to 1.0; this also means that stress and strain values will be roughly comparable). The upper bound on ρ in this and all the subsequent examples is $\overline{\rho} = 0.25$. The optimal weight was $V^* = 206.2$ and the maximal strain norm $e_{\max} = 2.76$, while the maximal stress norm was $\sigma_{\max} = 0.272$. These numbers will serve as reference numbers when defin-

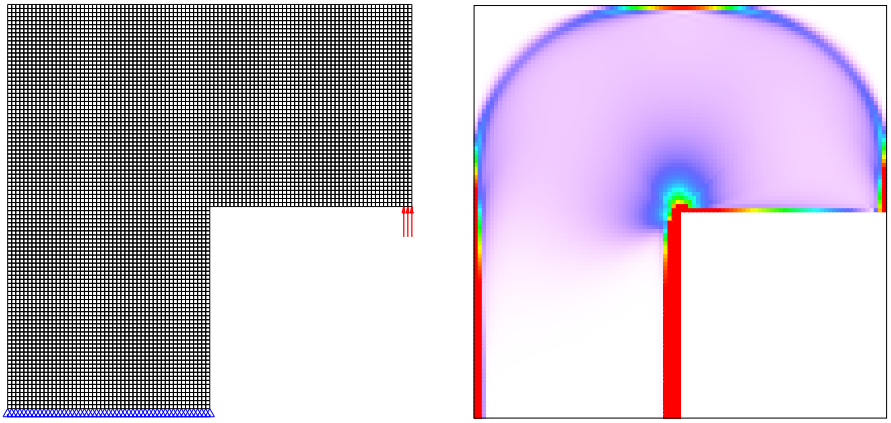

Figure 2: L-shaped domain: geometry, load and boundary conditions (left); VTS result without stress/strain constraints (right)

ing strain and stress upper bounds for this particular mesh. The maximum strain and stress was (as expected) located at the re-entrant corner.

Example 3.3 Let us now solve the strain constrained VTS problem (8) on the L-shaped domain from Example 3.2. The upper bound on strains was taken as $s_e = 1.0$. The solution obtained by PENNON was feasible, so the strain constraints were satisfied. The optimal weight for this problem was $V^* = 211.4$. Fig. 3(left) shows the optimal distribution of ρ, while the right-hand side of this figure presents the distribution of the strain norms. Compared to the unconstrained result, we indeed see change in the

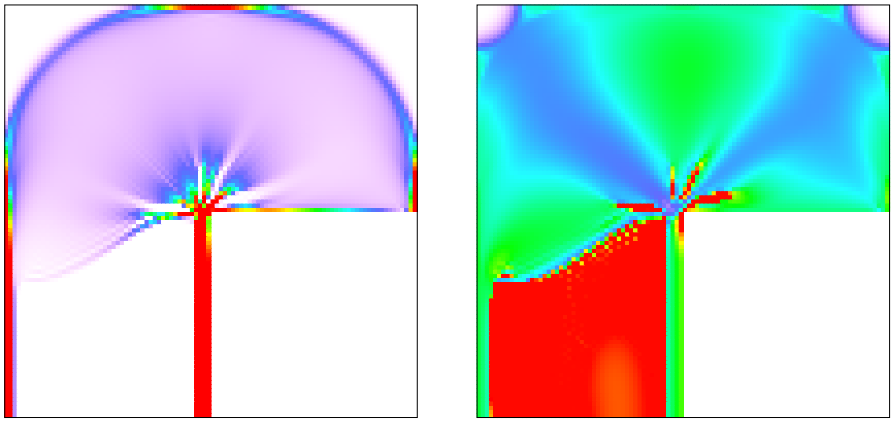

Figure 3: VTS formulation with strain constraints: optimal ρ (left) and optimal strain norms (right)

geometry of the optimal structure around the corner; this seems to indicate that we are on a right track. However, the optimal strains show the unwanted effect of "vanishing constraints": the strain constraints are mainly active for elements with (almost) zero ρ, i.e., for "holes".

To manage the problem of vanishing constraints, many authors propose to multiply both sides of the strain constraint by ρ_i. The constraint effect remains unchanged, the constraint will "vanish" for $\rho_i \to 0$ (this is what we want); however, the new problem becomes extremely hard to solve numerically (see [1] for more details). Instead, we replace the strain constraint in (8) by the following one

$$\rho_i^2 \sum_{k=1}^{nig} \|E_0 B_{i,k} u\|^2 \left[= \rho_i^2 u^T K_i u\right] \le s_\sigma \overline{\rho}^2, \quad i = 1, \ldots, m. \tag{10}$$

The physical interpretation of this constraint fully depends on the interpretation of ρ. For the "true" VTS problem, when ρ is the thickness of the structure, the left-hand side of (10) represents the (norm of the) internal force and the sense of such a constraint is questionable. However, when the thickness is considered constant and ρ is sort of "density" of the optimal material ρE_0, the left-hand side of (10) indeed measures the norm of the stress tensor. In any case, let us see what effect this new constraint has on the optimal structure.

Example 3.4 We solve the VTS problem with stress constraints (10) on the L-shaped domain from Example 3.2. The upper bound on stresses was again taken as

$$s_\sigma \overline{\rho}^2 = 1.0 \cdot \overline{\rho}^2 = 0.0625,$$

to get results comparable with Example 3.3. The optimal structure has weight $V^* = 210.9$. Fig. 4(left) shows the optimal distribution of ρ, and the right-hand side of this figure presents the distribution of the stress norms. This result is indeed "nicer" than that for the strain constraint. The sharp corner is replaced by a (approximation of) re-entrant semi-circle to avoid the stress concentration. Also, the active stress constraints are concentrated just around this corner.

When we decrease the upper bound to

$$s_\sigma \overline{\rho}^2 = 0.5 \cdot \overline{\rho}^2 = 0.03125,$$

we get a solution shown in Fig. 5 with optimal volume $V^* = 217.7$. The change in geometry is even more significant here. Moreover, looking at the stress norms, the constraints in almost all the elements on the "leg" from the re-entrant corner to the basis are active. This—and the high number of PENNON iterations—is a sign that we are almost on the border of feasibility and cannot decrease s_σ any more.

3.2 FMO with stress and strain constraints

Let us now turn to the primal subject of the paper, the free material optimization model. In the FMO problem, the strain constraints are defined analogously to the VTS prob-

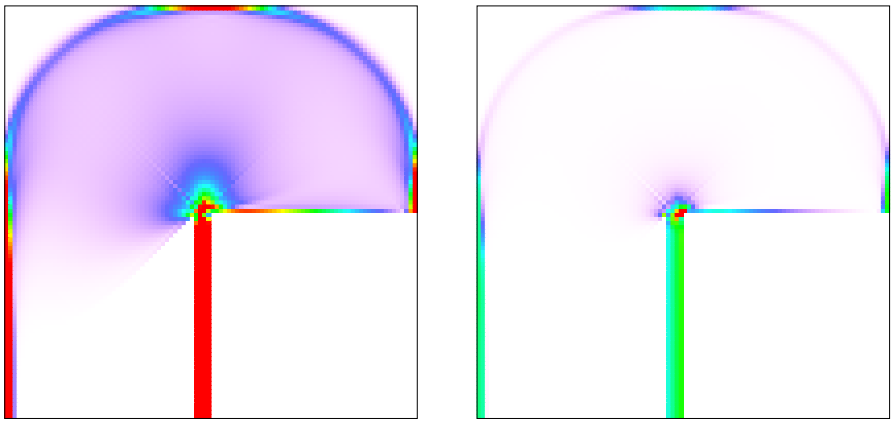

Figure 4: VTS formulation with stress constraints and $s_\sigma = 1.0$: optimal ρ (left) and optimal stress norms (right)

lem, leading to the strain constrained FMO problem

$$\min_{u,E} \sum_{i=1}^{m} \mathrm{Tr}(E_i) \tag{11}$$

subject to

$$\begin{aligned}
&E_i \succeq 0, \quad i = 1,\dots,m \\
&\underline{\rho} \leq \mathrm{Tr}(E_i) \leq \overline{\rho} \quad i = 1,\dots,m \\
&f^T u \leq \gamma \\
&A(E)u = f \\
&\sum_{k=1}^{nig} \|B_{i,k}u\|^2 \leq s_e, \qquad i = 1,\dots,m.
\end{aligned}$$

The stress in the FMO result is now also clearly defined by $\sigma = Ee$, hence the FMO problem with stress constraints reads as

$$\min_{u,E} \sum_{i=1}^{m} \mathrm{Tr}(E_i) \tag{12}$$

subject to

$$\begin{aligned}
&E_i \succeq 0, \quad i = 1,\dots,m \\
&\underline{\rho} \leq \mathrm{Tr}(E_i) \leq \overline{\rho} \quad i = 1,\dots,m \\
&f^T u \leq \gamma \\
&A(E)u = f \\
&\sum_{k=1}^{nig} \|EB_{i,k}u\|^2 \leq s_\sigma \overline{\rho}^2, \qquad i = 1,\dots,m.
\end{aligned}$$

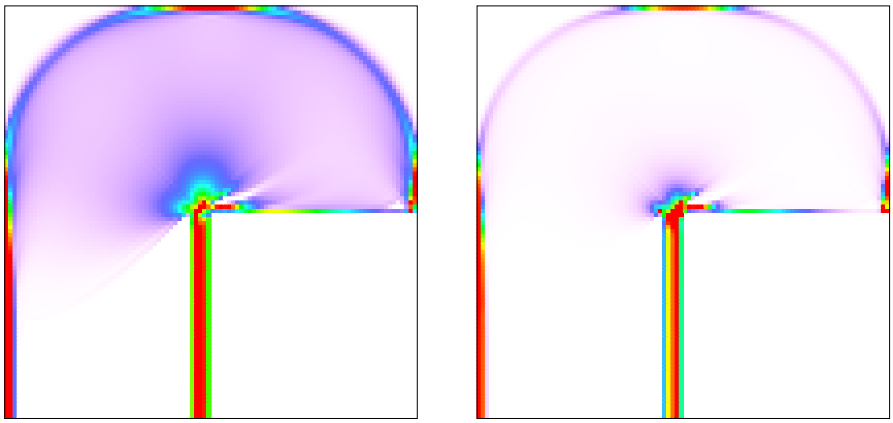

Figure 5: VTS formulation with stress constraints and $s_\sigma = 0.5$: optimal ρ (left) and optimal stress norms (right)

Both problems (11) and (12) are nonlinear semidefinite programming problems that can be solved by the variant of the code PENNON described in Section 4.

In the following, we will solve the above problems for the L-shaped domain from Example 3.2 with different values of the upper bounds and compare the results.

Remark 3.5 Before presenting the results, let us mention two most important facts that we have observed. First, the FMO model offers much more freedom than the VTS model, where the material properties were fixed. While in VTS the stress concentration had to be removed by change of geometry of the optimal structure, in the FMO case it can be treated *solely by the material properties around the re-entrant corner*.

Second, we observed a rather surprising fact that the optimal material was almost always orthotropic, notwithstanding the stress/strain constraints. This has been tested and confirmed a-posteriori for all examples and all elements. We do not see any theoretical reason that would explain this, but it allows us to plot the material directions of the optimal material and to better demonstrate its properties.

Example 3.6 We first solve the FMO problem without additional stress or strain constraints, to get reference values. The optimal structure, shown in Fig. 6 has volume 232.04 and the maximal stress and strain norm (7) is 0.202 and 3.456, respectively. We also evaluate the maximal values of the Tresca, von Mises, maximum stress and maximum strain failure criteria, computed at points of Gaussian integration.

We further solve the FMO problems (11) and (12) with stress and strain constraints. Table 1 shows the values of optimal volume and maximal stress, strain and failure criteria for examples with two different upper bounds, namely $s_\sigma = 1.0$, $s_\sigma = 0.7$ and $s_e = 1.0$, $s_e = 0.7$. Obviously, the maximal stress values were on their upper bound for the stress constrained problem, and, analogously, the maximal strains were on their upper bound for the strain constrained problem. The respective numbers are emphasized in the table. The presented numbers basically fulfill expectations up to one point.

On the one hand, the maximal stress in the strain constrained problem more or less coincides with that computed by the stress constrained problem (with the same value of the upper bound). On the other hand, the maximal strain in the stress constrained problem grows rapidly when we decrease the upper bound s_σ. That means that we have more freedom when solving the stress constrained problem. This is the effect of the vanishing constraints known already from the VTS problem: in the strain constrained problem we again restrict even elements that are not present in the optimal structure (see the figures below).

Because the strain constrained problem is more restrictive, we could not decrease the upper bound any more; the strain constrained problem would become infeasible. We can still, however, decrease the upper bound s_σ of the stress constrained problem. Table 2 shows the values for the stress constrained problem only, when s_σ goes down to 0.5.

As mentioned above, the strain constrained problem is more restrictive. Also, the strain constraints are active even in "white" regions, which is an unwanted effect. Note, however, that when we solve a strain constrained problem, the stresses in this problem are feasible in the stress constrained problem with the same upper bound. Hence, when we want to find a design satisfying stress constraints, we can solve the strain constrained problem (which can be numerically easier), keeping in mind that the resulting design actually satisfies tighter constraints and thus its cost function may be higher than optimal. This is apparent from Table 1.

Figures 6–17 present the corresponding distributions of optimal material stiffness, and optimal stress and strain norms. For each example, after presenting the optimal stiffness, we show detail of the optimal principal stress direction (and thus optimal material direction). We can see that in all cases the material around the re-entrant corner is composed of fibres making a smooth arc around the corner, thus preventing the stress singularity. The last two figures for each example show the optimal stress and strain distribution. Again, we can see that for the strain constrained problem, the constraints are often active at "white" regions with almost no material (see Figs. 11 and 15). On the other hand, the constraints of the stress constrained problem are always active just around the stress singularity or in regions with a stiff material.

4 The algorithm

The algorithm used in this article is based on a generalized augmented Lagrangian method for the solution of nonlinear (semidefinite) programs described in [8, 12]. Here we briefly recall it and show how it can be extended for the solution of the optimization problems introduced in Section 3.

The goal of the algorithm is to solve general nonlinear semidefinite optimization problems of the form

$$\begin{aligned} &\min_{x\in\mathbb{R}^n} f(x) \\ &\text{subject to} \\ &\qquad \mathscr{G}(x) \preccurlyeq 0; \end{aligned} \tag{13}$$

Table 1: FMO problem with stress or strain constraints

	no constr.	stress 1.0	strain 1.0	stress 0.7	strain 0.7
volume	228.62	230.53	230.81	232.43	233.90
stress	0.201	*0.0625*	0.0623	*0.04375*	0.0435
strain	3.431	20.15	*1.0*	15.3	*0.7*
Tresca	0.188	0.108	0.122	0.102	0.098
von Mises	0.0387	0.0142	0.0140	0.0107	0.0100
$\sigma_{\max}$	0.321	0.181	0.159	0.149	0.129
$e_{\max}$	1.347	2.674	0.727	2.240	0.600

Table 2: FMO problem with stress constraints

	no constr.	stress 1.0	stress 0.7	stress 0.5
volume	228.62	230.53	232.43	235.43
stress	0.201	*0.0625*	*0.04375*	*0.03125*
strain	3.431	20.15	15.3	32.34
Tresca	0.188	0.108	0.102	0.093
von Mises	0.0387	0.0142	0.0107	0.0092
$\sigma_{\max}$	0.321	0.181	0.149	0.123
$e_{\max}$	1.347	2.674	2.240	3.146

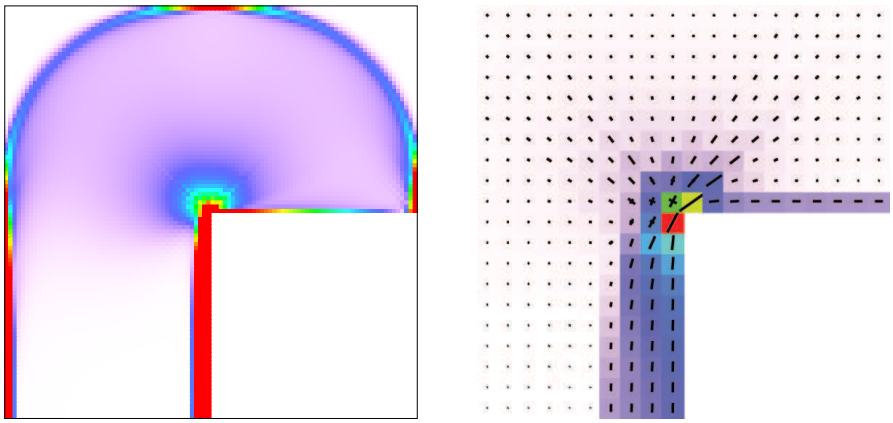

Figure 6: FMO formulation with no stress/strain constraints: optimal ρ (left) and optimal principal stress (right)

here $f : \mathbb{R}^n \to \mathbb{R}$ and $\mathscr{G}(x) : \mathbb{R}^n \to \mathbb{S}^m$ are twice continuously differentiable mappings and $\mathbb{S}^m$ is the space of symmetric $(m \times m)$-matrices.

The algorithm is based on a choice of a smooth modified barrier function $\Phi_p : \mathbb{S}^m \to \mathbb{S}^m$, depending on a parameter $p > 0$, that satisfies a number of assumptions (see [8]) guaranteeing, in particular, that

$$\mathscr{G}(x) \preccurlyeq 0 \Leftrightarrow \Phi_p(\mathscr{G}(x)) \preccurlyeq 0\,.$$

Thus for any $p > 0$, problem (13) has the same solution as the following "augmented" problem

$$\begin{aligned} &\min_{x \in \mathbb{R}^n} f(x) \\ &\text{subject to} \\ &\qquad \Phi_p(\mathscr{G}(x)) \preccurlyeq 0\,. \end{aligned} \tag{14}$$

A typical choice of Φ_p is

$$\Phi_p(\mathscr{G}(x)) = -p^2(\mathscr{G}(x) - pI)^{-1} - pI\,. \tag{15}$$

The Lagrangian of (14) can be viewed as a (generalized) augmented Lagrangian of (13):

$$F(x,U,p) = f(x) + \langle U, \Phi_p(\mathscr{G}(x))\rangle_{\mathbb{S}_m}\,; \tag{16}$$

here $U \in \mathbb{S}^m$ is a Lagrangian multiplier associated with the inequality constraint. The algorithm is defined as follows:

Algorithm 4.1 *Let x^1 and U^1 be given. Let $p^1 > 0, \alpha^1 > 0$. For $k = 1,2,\ldots$ repeat*

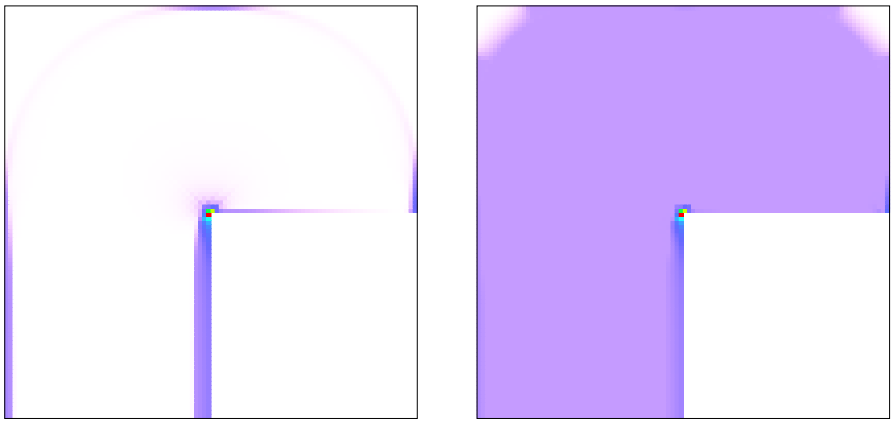

Figure 7: FMO formulation with no stress/strain constraints: optimal stress norms (left) and optimal strain norms (right)

until a stopping criterion is reached:

$$
\begin{aligned}
&(i) \qquad \text{Find } x^{k+1} \text{ satisfying } \|\nabla_x F(x^{k+1}, U^k, p^k)\| \leq \alpha^k \\
&(ii) \qquad U^{k+1} = D_{\mathscr{G}} \Phi_p(\mathscr{G}(x^{k+1}); U^k) \\
&(iii) \qquad p^{k+1} \leq p^k, \quad \alpha^{k+1} < \alpha^k .
\end{aligned}
$$

The unconstrained minimization problem in step (i) is approximately solved by modified Newton's method. Multiplier and penalty update strategies, as well as local and global convergence properties under standard assumptions are studied extensively in [12].

In the following we discuss how to solve optimization problems of type (11) and (12) (or the corresponding VTS problems) by variants of Algorithm 4.1. We offer two alternatives: a reduced and a direct approach.

Remark 4.2 Note that problem (14) covers problems with several matrix inequalities as well as problems subject to scalar inequality constraints of the form

$$g_i(x) \leq 0, \qquad i = 1, 2, \ldots, k.$$

Writing the augmented Lagrangian explicitly for this case, we obtain:

$$
\begin{aligned}
F(x, U, w, p) \quad = \quad & f(x) + \sum_{i=1}^{l} \langle U_i, \Phi_p(\mathscr{G}_i(x)) \rangle_{\mathbb{S}_m} \\
& + \sum_{i=1}^{k} w_i \varphi_p(g_i(x))
\end{aligned}
$$

where φ is the scalar version of Φ and $w \in \mathbb{R}^k$ the associated multiplier.

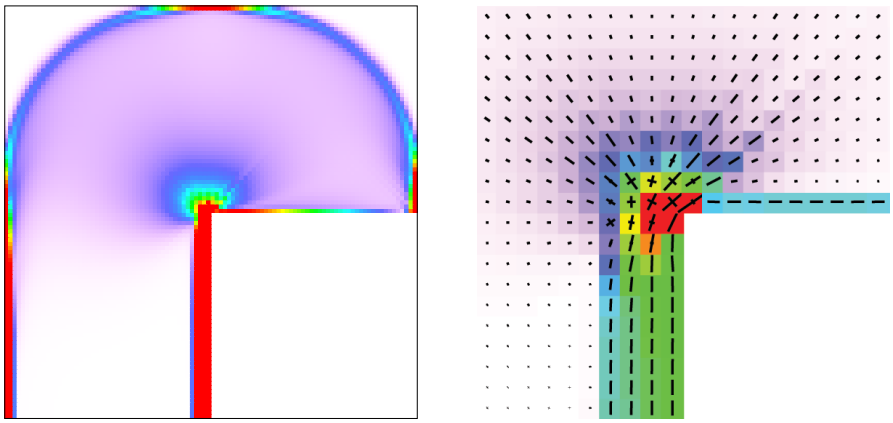

Figure 8: FMO formulation with stress constraints, $s_\sigma = 1.0$: optimal ρ (left) and optimal principal stress (right)

4.1 The reduced approach

Many approaches for the solution of optimal design problems are based on reduced formulations, which are solely defined in the design variables. Often the reduced problems are solved by first order optimization algorithms, where the calculations of the first order derivatives are based on solutions of adjoint problems. In this section we want to describe a similar approach. However, rather than restricting ourselves to a first order algorithm, we will demonstrate how second order derivatives can be efficiently calculated and exploited by a variant of Algorithm 4.1.

We start with the derivation of reduced formulations for problems (11) and (12). It is easily seen that for positive $\underline{\rho}$ the stiffness matrix $A(E)$ is positive definite. Thus we can eliminate the state variable u by substituting $u := A(E)^{-1}$ and formulate the reduced problems

$$\min_E \sum_{i=1}^{m} \mathrm{Tr}(E_i) \tag{17}$$

subject to

$$\begin{aligned}
&E_i \succeq 0, \quad i = 1,\dots,m \\
&\underline{\rho} \le \mathrm{Tr}(E_i) \le \overline{\rho}, \quad i = 1,\dots,m \\
&f^T (A(E))^{-1} f \le \gamma \\
&\sum_{k=1}^{nig} \|B_{i,k}(A(E))^{-1} f\|^2 \le s_e, \qquad i = 1,\dots,m
\end{aligned}$$

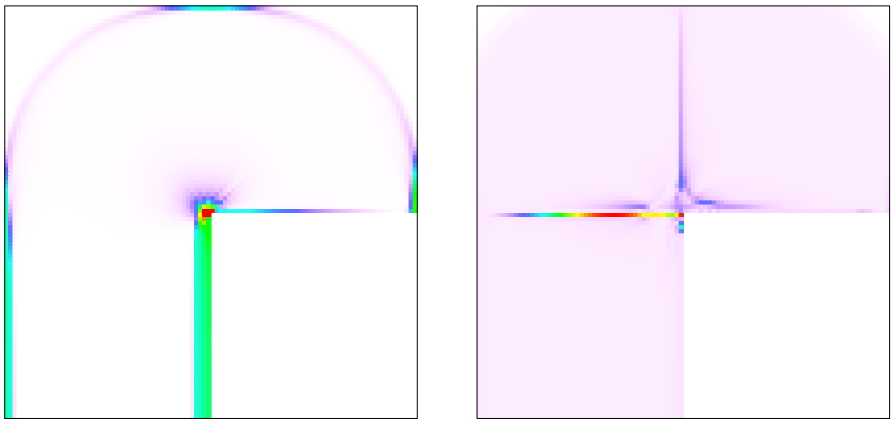

Figure 9: FMO formulation with stress constraints, $s_\sigma = 1.0$: optimal stress norms (left) and optimal strain norms (right)

and

$$\min_{E} \sum_{i=1}^{m} \mathrm{Tr}(E_i) \tag{18}$$

subject to

$$\begin{aligned}
& E_i \succeq 0, \quad i = 1,\ldots,m \\
& \underline{\rho} \le \mathrm{Tr}(E_i) \le \overline{\rho}, \quad i = 1,\ldots,m \\
& f^T (A(E))^{-1} f \le \gamma \\
& \sum_{k=1}^{nig} \|E B_{i,k} (A(E))^{-1} f\|^2 \le s_\sigma \overline{\rho}^2, \qquad i = 1,\ldots,m.
\end{aligned}$$

Obviously, both problems are instances of the general optimization problem (13). Nevertheless it is not recommendable to apply Algorithm 4.1 directly. The reason is twofold: First, the Hessian of the augmented Lagrangian associated with problems (17) and (18) is a large dense matrix and the algorithm may run out of memory. Second, Algorithm 4.1 does not maintain the feasibility of inequalities strictly throughout the optimization process. Consequently, the global stiffness matrix could become indefinite and the algorithm may fail.

The first issue can be resolved by the use of approximate Newton's method for the solution of step (i) in Algorithm 4.1. Recently, the authors have successfully implemented and tested a version of Algorithm 4.1, where the solution of the Newton system is based on Krylov type methods (see [9]). Instead of calculating the full Hessian of the augmented Lagrangian F, this algorithm requires just Hessian-vector products. Below we demonstrate how such a product can be calculated in an efficient way for the problems considered in this paper.

In order to get rid of the second difficulty mentioned above, we treat the inequali-

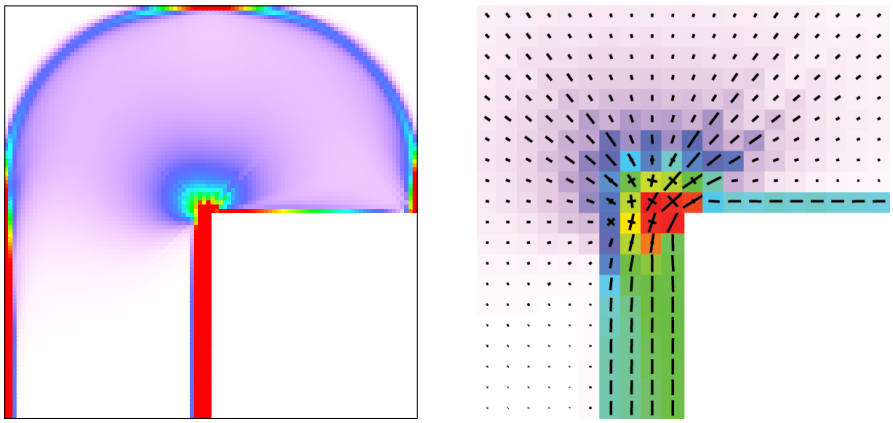

Figure 10: FMO formulation with strain constraints, $s_e = 1.0$: optimal ρ (left) and optimal principal stress (right)

ties that should be strictly feasible during the optimization process by a classic barrier function. For this reason we introduce an additional matrix inequality

$$\mathscr{S}(x) \preccurlyeq 0$$

in problem (14) and define the augmented Lagrangian

$$\widetilde{F}(x,U,p,s) = f(x) + \langle U, \Phi_p(\mathscr{G}(x))\rangle_{\mathbb{S}_m} + s\Phi_{\text{bar}}(\mathscr{S}(x)), \tag{19}$$

where Φ_{bar} can be defined, for example, by

$$\Phi_{\text{bar}}(\mathscr{S}(x)) = -\log\det(-\mathscr{S}(x)).$$

We thus obtain the following algorithm:

Algorithm 4.3 *Let x^1 and U^1 be given. Let $p^1 > 0, s^1 > 0, \alpha^1 > 0$. For $k = 1,2,\ldots$ repeat until a stopping criterion is reached:*

$$\begin{aligned}
&(i) && \text{Find } x^{k+1} \text{ satisfying } \|\nabla_x \widetilde{F}(x^{k+1},U^k,p^k,s^k)\| \le \alpha^k \\
&(ii) && U^{k+1} = D_{\mathscr{G}}\Phi_p(\mathscr{G}(x^{k+1});U^k) \\
&(iii) && p^{k+1} \le p^k, \quad s^{k+1} < s^k, \quad \alpha^{k+1} < \alpha^k.
\end{aligned}$$

Note that, while the penalty parameter p^k maybe constant from a certain index $\bar{k}$ (see again [12] for details), the barrier parameter is required to tend to zero with increasing k.

Remark 4.4 (Complexity estimates) We consider the reduced VTS problem with strain

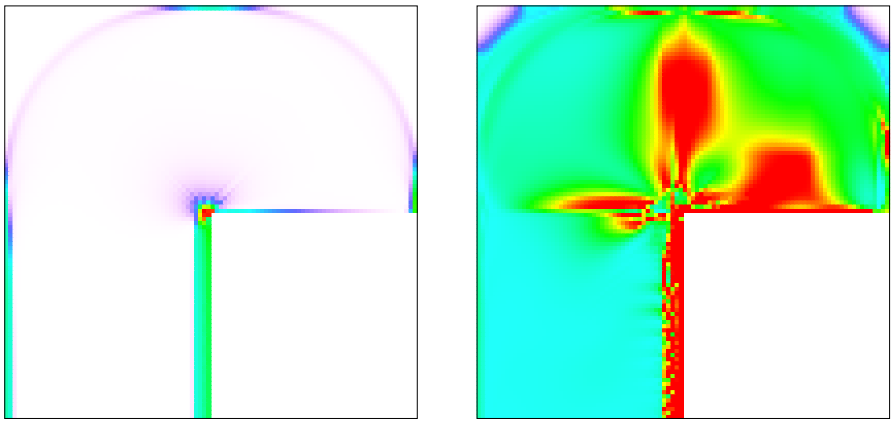

Figure 11: FMO formulation with strain constraints, $s_e = 1.0$: optimal stress norms (left) and optimal strain norms (right)

constraints

$$\min_{\rho} \sum_{i=1}^{m} \rho_i \tag{20}$$

subject to

$$\begin{aligned} &\underline{\rho} \leq \rho_i \leq \overline{\rho} \quad i = 1,\ldots,m \\ &f^T (A(\rho))^{-1} f \leq \gamma \\ &f^T (A(\rho))^{-1} A_i (A(\rho))^{-1} f \leq s_e,\ i = 1,\ldots,m, \end{aligned}$$

where $A(\rho) = \sum_{i=1}^{m} \rho_i A_i(E_0)$ and $A_i = \sum_{k=1}^{nig} B_{i,k}^T B_{i,k}$. Using the abbreviation $g_0(\rho) = f^T (A(\rho))^{-1} f$ and

$$g_i(\rho) = f^T (A(\rho))^{-1} A_i (A(\rho))^{-1} f$$

for $i = 1,\ldots,m$ and neglecting the lower and upper bounds on ρ, the Hessian of the augmented Lagrangian associated with problem (20) can be written as

$$\nabla^2_{\rho\rho} F(\rho, w, p) = \sum_{k=0}^{m} \alpha_k \nabla^2_{\rho\rho} g_k(\rho) + \sum_{k=0}^{m} \beta_k \nabla_\rho g_k(\rho) \nabla_\rho g_k(\rho)^\top,$$

where the coefficients α_k, β_k, $k = 0,\ldots,m$, depend on the penalty function φ, the design variable ρ and the Lagrangian multipliers w. Setting $u := A(\rho)^{-1} f$, one can verify that for a vector $d \in \mathbb{R}^n$ the matrix-vector product

$$\sum_{k=1}^{m} \beta_k \nabla_\rho g_k(\rho) \nabla_\rho g_k(\rho)^\top \cdot d \tag{21}$$

is given by the formula

$$2 \left(u^T \left(\sum \gamma_k \beta_k A_k \right) A(\rho)^{-1} \right) A_l u,\ l = 1,\ldots,m,$$

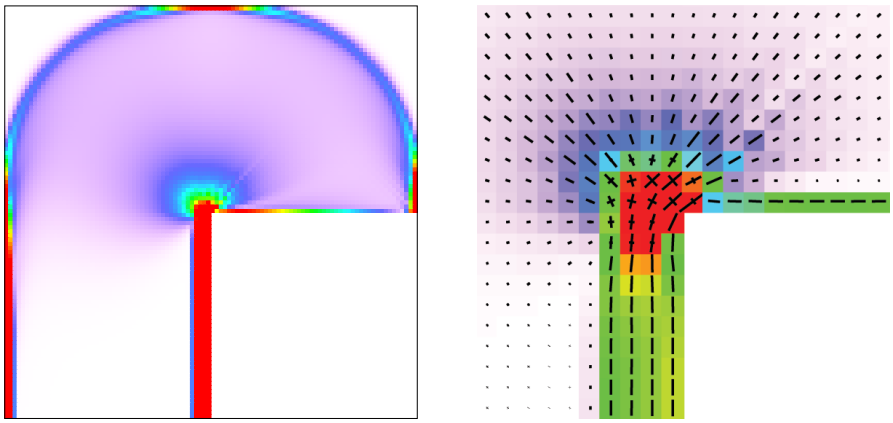

Figure 12: FMO formulation with stress constraints, $s_\sigma = 0.7$: optimal ρ (left) and optimal principal stress (right)

where

$$\gamma_k = u^T A_k \left(A(\rho)^{-1} \left(\sum d_j A_j\right) u\right), \; k = 1, \ldots, m.$$

Performing the calculations in a convenient order and assuming that

- the matrices A_i are sparsely populated with $O(1)$ entries,
- K is the maximal number of nonzero entries per row in the stiffness matrix $A(\rho)$,

we obtain the complexity formula $O(m+Kn)$ for the calculation of (21). In a similar way, we can show that the matrix-vector product

$$\sum_{k=0}^{m} \alpha_k \nabla^2_{\rho\rho} g_k(\rho) \cdot d$$

can be assembled as a sum of terms of the type

$$\left(u^T \left(\sum \alpha_k A_k\right) A(\rho)^{-1}\right) A_l \left(A(\rho)^{-1} \left(\sum d_k A_k\right) u\right), \; l = 1, \ldots, m$$

in $O(m+Kn)$ steps. Finally, taking into account that

- a multiplication of the Hessian of the compliance constraint with a vector $d \in \mathbb{R}^n$ requires also $O(m+Kn)$ steps and that
- the computational complexity of the factorization of the stiffness matrix is usually given by $O(m+Kn^2)$,

we can conclude that the computational effort for the solution of problem (20) is of the same order as the computational effort for the solution of the reduced form of problem (5), provided the number Hessian-vector multiplications required is not influenced in

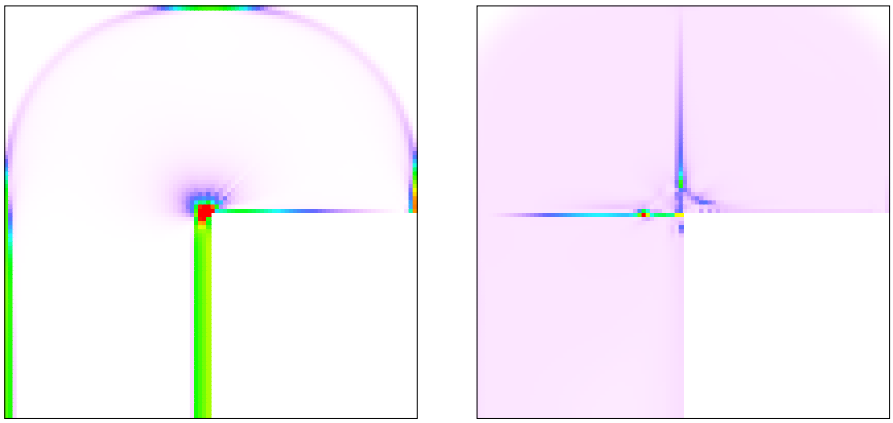

Figure 13: FMO formulation with stress constraints, $s_\sigma = 0.7$: optimal stress norms (left) and optimal strain norms (right)

a negative way by the strain constraints. This seems to make the reduced approach attractive, as the reduced form of problem (5) is successfully solved in practice.

We have decided to derive the complexity estimates using problem (20) in order to keep the notation as simple as possible. Note however, that comparable estimates can be derived for problems (17) and (18).

4.2 The direct approach

As an alternative to the reduced approach presented in the preceding section, one can try to solve problems (11) and (12) directly. An immediate approach is to rewrite the system of bilinear equations

$$A(E)u = f$$

arising from the equilibrium constraint by inequalities and attempt to solve the resulting problem by Algorithm 4.1. Unfortunately, our numerical experience showed that such an approach is not only rather inefficient, but fails completely in most cases. However, during our numerical experiments we made the following useful observation: The algorithm behaved stable as long as

- the material matrices stayed strictly positive definite
- the equilibrium equation was only slightly violated.

These observations motivated the following modifications: First, we decided to treat the matrix inequalities $E_i \succeq 0$, $i = 1, \ldots, m$, again by the classic barrier approach (compare Section 4.1) and set $\underline{\rho} = 10^{-6}$. Second, we changed the concept of equality handling in our algorithm. More precisely, we adopted a concept which is successfully used in modern primal-dual interior point algorithms (see, e.g., [14, 13]): rather than using augmented Lagrangians, we handle the equality constraints directly on the level

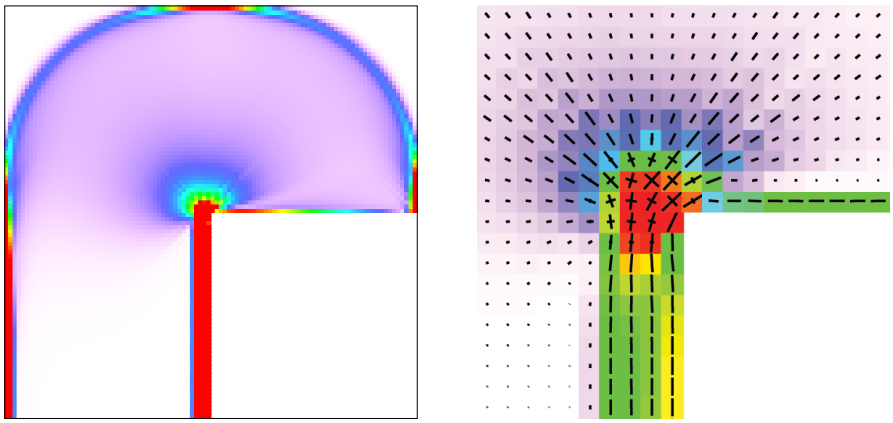

Figure 14: FMO formulation with strain constraints, $s_e = 0.7$: optimal ρ (left) and optimal principal stress (right)

of the subproblem. This leads to the following approach. Consider the optimization problem

$$\begin{aligned} &\min_{x\in\mathbb{R}^n} f(x) \\ &\text{subject to} \\ &\qquad \mathscr{G}(x) \preccurlyeq 0\,, \\ &\qquad \mathscr{S}(x) \preccurlyeq 0\,, \\ &\qquad h(x) = 0\,, \end{aligned} \tag{22}$$

where f, $\mathscr{G}$ and $\mathscr{S}$ are defined as in the previous sections and $h : \mathbb{R}^n \to \mathbb{R}^d$ represents a set of equality constraints. Then we define the augmented Lagrangian

$$\begin{aligned} &\overline{F}(x,U,v,p,s) = \\ &f(x) + \langle U, \Phi_p(\mathscr{G}(x))\rangle_{\mathbb{S}_m} + s\Phi_{\text{bar}}(\mathscr{S}(x)) + v^\top h(x)\,, \end{aligned} \tag{23}$$

where $U, \Phi, \Phi_{\text{bar}}, p, s$ are defined as before and $v \in \mathbb{R}^d$ is the vector of Lagrangian multipliers associated with the equality constraints. Now, on the level of the subproblem, we attempt to find an approximate solution of the following system (in x and v):

$$\begin{aligned} \nabla_x \overline{F}(x,U,v,p,s) = 0\,, \\ h(x) = 0\,, \end{aligned} \tag{24}$$

where the penalty and barrier parameters s, p, as well as the multiplier U are fixed. In order to solve systems of type (24), we apply the damped Newton method. Descent directions are calculated utilizing the factorization routine MA27 from the Harwell subroutine library ([5]) in combination with an inertia correction strategy as described in [14]. Moreover, the step length is derived using an augmented Lagrangian merit

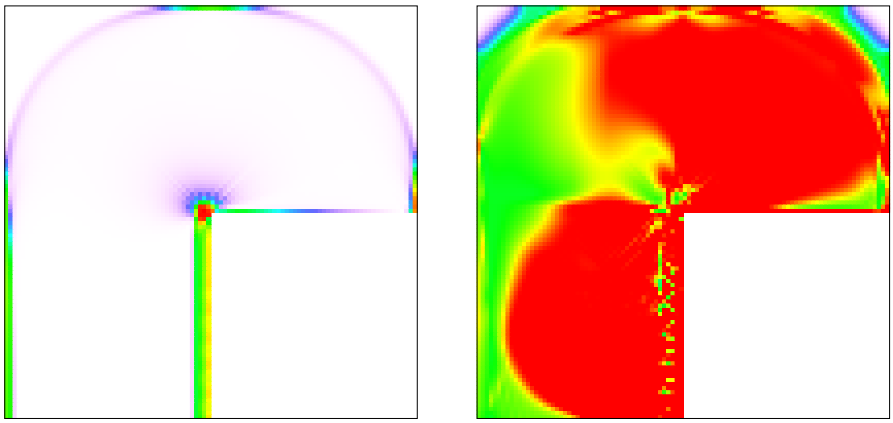

Figure 15: FMO formulation with strain constraints, $s_e = 0.7$: optimal stress norms (left) and optimal strain norms (right)

function defined as

$$\overline{F}(x,U,v,p,s) + \frac{1}{2\mu}\|h(x)\|_2^2$$

along with an Armijo rule. Now we are prepared to state the modified algorithm:

Algorithm 4.5 *Let x^1, U^1 and v_1 be given. Let $p^1 > 0, s^1 > 0, \alpha^1 > 0$. For $k = 1,2,\ldots$ repeat until a stopping criterion is reached:*

$$\begin{aligned}
&(i) \qquad \text{Find } x^{k+1}, v^{k+1} \text{ satisfying} \\
&\qquad\qquad \|\nabla_x \overline{F}(x^{k+1}, U^k, v^{k+1}, p^k, s^k)\| \le \alpha^k \\
&\qquad\qquad \|h(x^k)\| \le \alpha^k \\
&(ii) \qquad U^{k+1} = D_{\mathscr{G}}\Phi_p(\mathscr{G}(x^{k+1}); U^k) \\
&(iii) \qquad p^{k+1} \le p^k, \quad s^{k+1} < s^k, \quad \alpha^{k+1} < \alpha^k .
\end{aligned}$$

4.3 Which approach is preferable?

So far we have only implemented the direct algorithm developed in Section 4.2. Consequently, all numerical studies presented in Section 3 were computed by this approach. The main reason for our decision was that the modifications to our optimization software package PENNON needed for the direct approach are useful for a much wider class of optimization problems as the one presented in this article. Another reason was that we could extend an existing AMPL interface (see [7]) of PENNON, which enabled us to define optimization problems (11) and (12) in a comfortable way. The third reason was that very preliminary experiments on a closely related class of structural optimization problems (FMO problems with displacement constraints) resulted in a high number of Hessian-vector products needed in the reduced approach. However, the structure of the

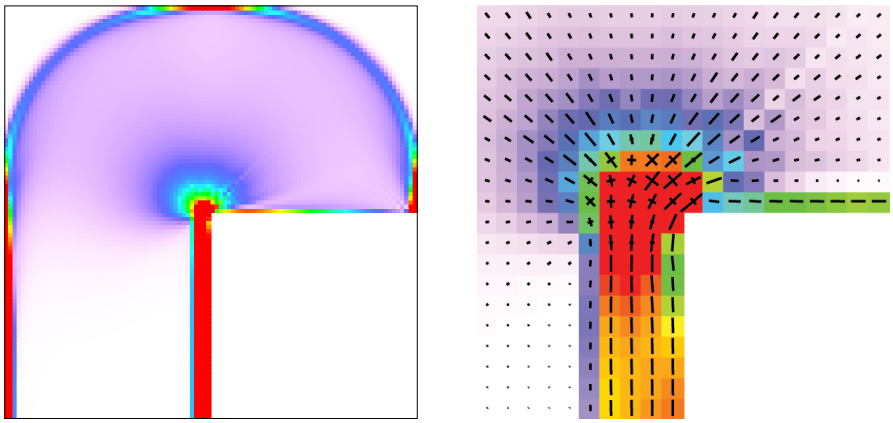

Figure 16: FMO formulation with stress constraints, $s_\sigma = 0.5$: optimal ρ (left) and optimal principal stress (right)

problems discussed in this paper is different, so we cannot draw a final conclusion on which algorithm is preferable in practice at this point of time.

acknowledgement

The work was partially done while MK was visiting the Department of Mathematics, Technical University of Denmark, Kgs. Lyngby, Denmark. The support and hospitality of this institution is gratefully acknowledged.

References

[1] W. Achtziger and Ch. Kanzow. Mathematical programs with vanishing constraints: Optimality conditions and constraint qualifications. Technical Report No. 263, Institute of Applied Mathematics and Statistics, University of Würzburg, Germany, 2005.

[2] A. Ben-Tal, M. Kočvara, A. Nemirovski, and J. Zowe. Free material design via semidefinite programming. The multi-load case with contact conditions. *SIAM J. Optimization*, 9:813–832, 1997.

[3] M. P. Bendsøe, J. M. Guades, R.B. Haber, P. Pedersen, and J. E. Taylor. An analytical model to predict optimal material properties in the context of optimal structural design. *J. Applied Mechanics*, 61:930–937, 1994.

[4] P. G. Ciarlet. *The Finite Element Method for Elliptic Problems*. North-Holland, Amsterdam, New York, Oxford, 1978.

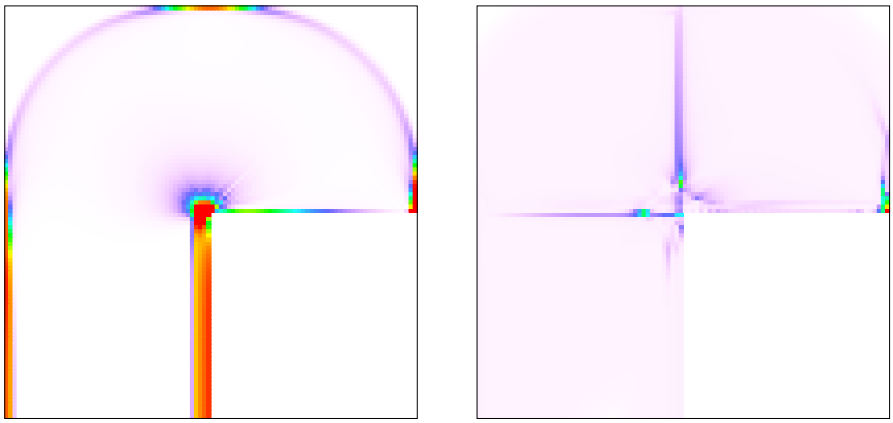

Figure 17: FMO formulation with stress constraints, $s_\sigma = 0.5$: optimal stress norms (left) and optimal strain norms (right)

[5] I. S. Duff and J. K. Reid. MA27—A set of Fortran subroutines for solving sparse symmetric sets of linear equations. Tech. Report R.10533, AERE, Harwell, Oxfordshire, UK, 1982.

[6] P. Duysinx and M. P. Bendsøe. Topology optimization of continuum structures with local stress constraints. *Int. J. Numer. Methods Eng.*, 43:1453–1478, 1998.

[7] R. Fourer, D. M. Gay, and B. W. Kernighan. AMPL: A modeling language for mathematical programming. *The Scientific Press, South San Francisco*, 1993.

[8] M. Kočvara and M. Stingl. PENNON—a code for convex nonlinear and semidefinite programming. *Optimization Methods and Software*, 18(3):317–333, 2003.

[9] M. Kočvara and M. Stingl. On the solution of large-scale SDP problems by the modified barrier method using iterative solvers. *Math. Program., Ser. B,*, 2006. To appear.

[10] M. Kočvara and J. Zowe. Free material optimization: An overview. In A.H. Siddiqi and M. Kočvara, editors, *Trends in Industrial and Applied Mathematics*, pages 181–215. Kluwer Academic Publishers, Dordrecht, 2002.

[11] R. Lipton and M. Stuebner. Inverse homogenization and design of microstructure for pointwise stress control. *Quart. J. Mech. and Appl. Maths.*, 59:139–161, 2006.

[12] M. Stingl. *On the Solution of Nonlinear Semidefinite Programs by Augmented Lagrangian Methods*. PhD thesis, Institute of Applied Mathematics II, Friedrich-Alexander University of Erlangen-Nuremberg, 2005.

[13] R. J. Vanderbei and D. F. Shanno. An interior point algorithm for nonconvex nonlinear programming. *Computational Optimization and Applications*, 13:231–252, 1999.

[14] A. Wächter and L. T. Biegler. On the implementation of a primal-dual interior point filter line search algorithm for large-scale nonlinear programming. *Math. Prog.*, 106:25–57, 2006.

[15] J. Zowe, M. Kočvara, and M. Bendsøe. Free material optimization via mathematical programming. *Math. Prog., Series B*, 79:445–466, 1997.